https://doi.org/10.20965/ijat.2016.p0030

Paper:

Surface Texturing in Micro Parametric Machining

Takashi Matsumura, Yasuharu Hayase, Jerome Blanchet, Naoki Iioka, and Ryo Kato

Tokyo Denki University
5 Senjyu Asahi-cho, Adachi-ku, Tokyo, 120-8551, Japan
E-mail: tmatsumu@cck.dendai.ac.jp

[Received August 18, 2015; accepted December 7, 2015]

Parametric machining is applied to fabricate microscale textures on surfaces by rotating the workpiece and tool. Periodic circular textures are controlled by only four parameters: the distance from the rotation center of the workpiece to that of the tool holder, the rotation radius of the tool in the tool holder, and the angular velocities of the workpiece and the tool holder. The textures to be machined are controlled by simulating the trajectory of the tool on the workpiece. A texturing machine was developed with two servomotors and three stepping motors, where the rotations of the servomotors were synchronized. Some examples are shown to verify the presented texturing in cutting tests. Because functional surfaces should be controlled by the surface structure, a model is presented to simulate the surface profiles of the textures. The orientation of the cutting tool with respect to the cutting direction is discussed in terms of the surface structure and the surface finish. The cutting load is estimated with the indentation and the shearing components in a simplified force model.

Keywords: cutting, texturing, surface profile, cutting force, micro machining

1. Introduction

Functional surfaces are used to control the physical, chemical, or physicochemical properties at the interfaces between substances in several industries. Surface functions have conventionally been controlled by the material properties, such as the coating of the surfaces with thin layers. Some surface functions, such as wettability, can be artificially controlled by changing the surface topography [1, 2].

Many studies have been conducted on surface texturing for diverse applications [3]. One application of surface structures is in manipulating the tribological properties of a surface. Because the friction coefficient depends on the surface roughness, friction at an interface of substances is controlled by the surface structure at the interface. One structured surface using microscale dimples has been fabricated by abrasive jet, excimer laser beam, or reactive ion etching to maintain lubrication at the interface [4, 5]. The microscale dimples are effective in controlling the friction coefficient [6]. Surfaces were successfully textured by laser processing to control solid lubrication on the surface [7]. Microscale dimples were also fabricated in laser coating-texturing and improved the abrasive wear resistance of a material [8]. A CO_2 laser-beam modulation was applied to machine the microscale dimples on the roll surfaces of one component with a rotating polygon [9].

Although chemical or energy-beam processes can be used to manufacture surface structures, some issues require improvement regarding the environmental impact, flexibility, cost, and production rate. Micromechanical machining is one proposed alternative process for manufacturing functional surfaces. When microscale structures are fabricated on surfaces by micromachining with numerical control, controllable functional surfaces such as functionally graded and integrated surfaces can be manufactured [10]. Microstructures have been successfully machined by microscale molding and forming to control wettability [11]. Microscale dimples were formed mechanically by pellet-pressing and found to improve the tribological properties of the substrate [12]. The widths and depths of the dimples were controlled by changing the press load. Whirling has also been applied to form microscale dimples at high machining rates [13]. Microscale dimples were machined with a ball-end mill on both flat and cylindrical surfaces [14, 15]. A force model has been presented for the machining of dimples. After this development, microscale asperities were manufactured on surfaces to investigate the friction coefficients in injection molding using microscale dimpled surfaces [16]. Dimpled surfaces machined by milling were applied to control the reflection range [17].

In microscale cuttings, extensive numerical control (NC) data are required to fabricate the large-area surface structures required for practical use. Interpolation in digital control deteriorates the machining accuracy. This study presents a parametric microscale cutting for fabrication of periodic circular textures on surfaces to control friction at the interfaces between substances. Parametric micro cutting was applied to manufacture microscale channels on glass plates by the simultaneous control of rotational and linear motions [18]. In this study, microscale grooves are machined by synchronized rotations of the cutting tool and workpiece. The presented process is

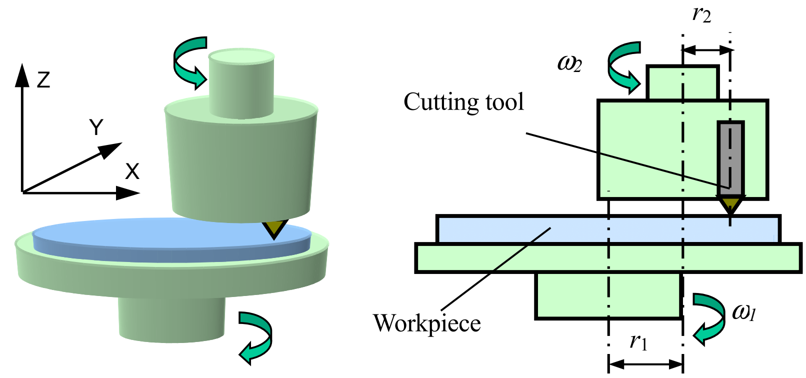

(a) Operation (b) Parameters in texturing

Fig. 1. Parametric texturing.

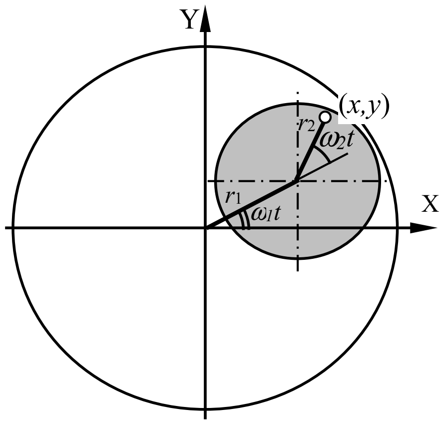

Fig. 2. Analysis of tool motion.

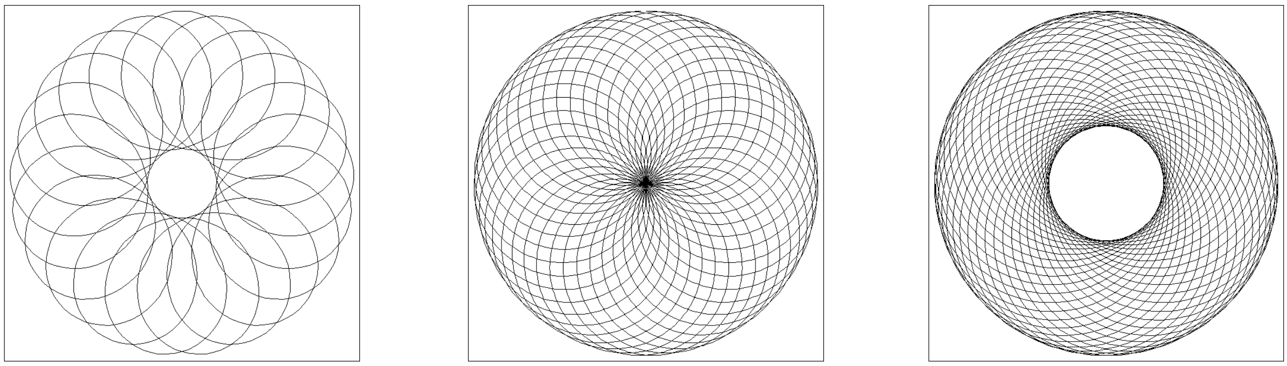

(a) $r_1 > r_2$ (b) $r_1 = r_2$ (c) $r_1 < r_2$

Fig. 3. Simulation of textured pattern.

controlled by a small number of parameters, based on the principle of spiral graphing. A mathematical model for the cutting is presented to simulate the machining patterns resulting from specific control parameters. A machine was developed to fabricate the surface textures; machining tests were conducted to verify the presented cutting manner with the simulation. A surface structure model is presented to demonstrate the control of the structure shape and alignment by adjusting the machining parameters. The surface finish is discussed in terms of tool geometry. In microscale cuttings, the cutting forces must be estimated to determine the cutting parameters. The cutting force of an aluminum alloy is also discussed with a model integrating indentation and shearing deformation modes. Finally, the cutting force in the presented texturing is simulated using the determined force model.

2. Parametric Machining

Figure 1 shows the parametric texturing with synchronized rotations of the tool and the workpiece. The parameters controlling the texturing, shown in **Fig. 1(b)**, are as follows:

(1) The distance r_1 between the center of the tool holder and that of the workpiece rotation

(2) The distance r_2 between the tool and the center of the tool holder

(3) The angular velocity ω_1 of workpiece rotation

(4) The angular velocity ω_2 of the tool holder rotation

Table 1. Control parameters.

	Condition A $r_1 > r_2$	Condition B $r_1 = r_2$	Condition C $r_1 < r_2$
r_1	6mm	4mm	2mm
r_2	4mm		
ω_1	0.628 rad/sec (6rpm)		
ω_2	25.12 rad/sec (240rpm)		

In the texturing, the workpiece rotates slowly as the tool rotates at set speed in actual cutting. The texture patterns can be analyzed in the model shown in **Fig. 2**, where the center of the tool rotation rotates around the workpiece with the tool holder. The trajectory of the tool is expressed as the following functions of time t:

$$\left.\begin{array}{l} x = r_1 \cos(\omega_1 t) + r_2 \cos\{(\omega_1 + \omega_2)t\} \\ y = r_1 \sin(\omega_1 t) + r_2 \sin\{(\omega_1 + \omega_2)t\} \end{array}\right\} \quad . . \quad (1)$$

Figure 3 shows examples of the simulated patterns based on Eq. (1) with changing r_1, with control parameters as shown in **Table 1**. The presented texturing fabri-

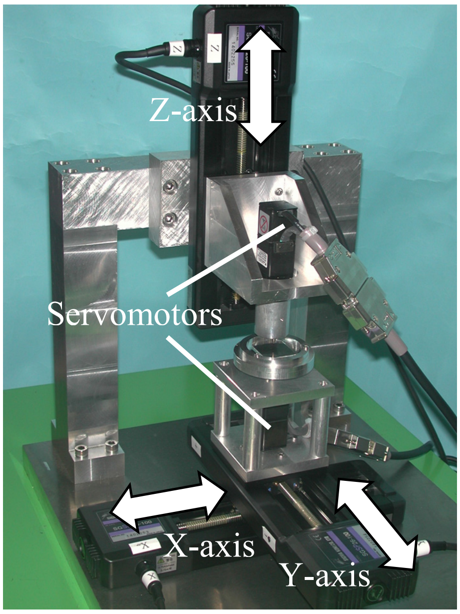

Fig. 4. Micro-texturing machine.

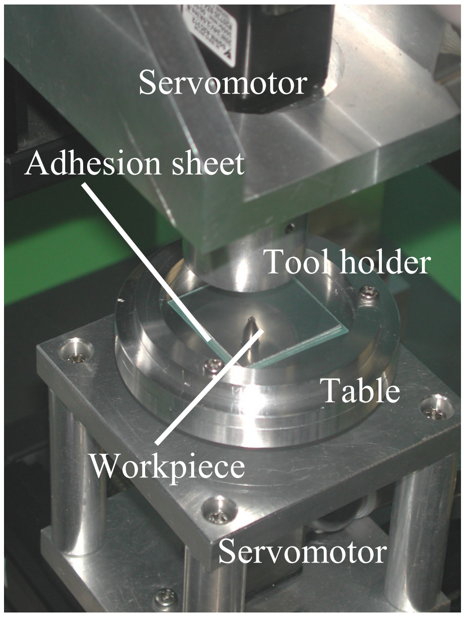

Fig. 5. Workpiece set in work area.

cates periodic circular structures on the surfaces based on mathematical equations. Typically, exhaustive NC data are required to fabricate the large-area patterns used in practice. In the presented texturing method, the surface structures are controlled by only four parameters, with no NC programs. More accurate curved structures are fabricated by this analog control manner than by the cutting process controlled by digital interpolation. Because the periodic textures are controlled by rotational motions, textures including linear patterns cannot be machined by this approach, which is one limitation. The texture is controlled in the X-Y plane by Eq. (1) for a specified cutting depth. Therefore, textures can only be formed on flat surfaces, and not on free-form surfaces.

3. Micro-Texturing Machine

Based on the texturing principle described, a micro-texturing machine was developed to machine microscale grooves by cutting, as shown in **Fig. 4**. The rotation of the workpiece and that of the tool holder are controlled simultaneously with a resolution of 0.01° by two servomotors. The cutting tool is mounted on the tool holder at a distance of 4 mm from the center of the rotation, as shown in **Fig. 1(b)**. The rotation center of the tool holder is controlled relative to that of the workpiece by linear stages. The linear stages are driven by stepping motors with a resolution of 1 μm. A heat-peelable pressure-sensitive adhesive sheet is used to clamp the workpiece, as shown in **Fig. 5**. The workpiece can be easily peeled by heating to above 90°C. The presented texturing requires high alignment accuracy for the machining of grooves with uniform depth. The machine was polished using alumina mineral paste to adjust the alignment of the workpiece relative to the tool before cutting.

Fig. 6. Single-crystal diamond tool.

4. Machining Example

Cutting tests were conducted to verify the presented texturing on aluminum alloy (A5056) plates of 30 mm × 30 mm × 1 mm dimensions using the cutting parameters in **Table 1**, which are identical to those of the simulation in **Fig. 3**. **Fig. 6** shows the employed cutting tool using a pyramid-shaped single-crystal diamond tip. A cutting depth of 1 μm was applied incrementally for each rotation of the workpiece. The total cutting depth was 30 μm after 30 workpiece rotations. The contact of the tool and workpiece surface was detected by observation with a charge-coupled device (CCD) camera. Cutting oil was supplied to reduce the adhesion of substrate chips to the tool. **Fig. 7** shows examples of the machined textures with changes in the distance r_1. The presented texturing method based on Eq. (1) is verified by comparing the machined patterns with the simulations shown in **Fig. 3**.

In order to determine the effect of polishing for the adjustment of the tool-workpiece alignment, texturing was also performed without polishing. **Fig. 8** shows an ex-

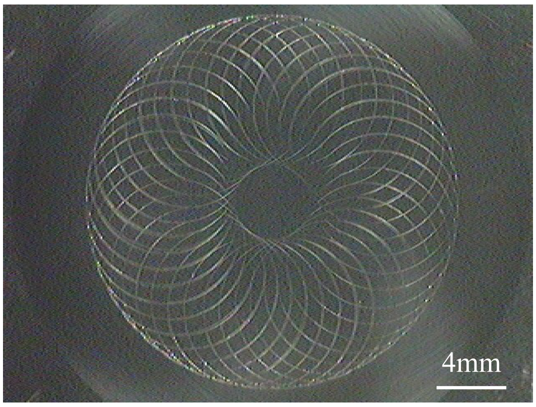

(a) $r_1 > r_2$

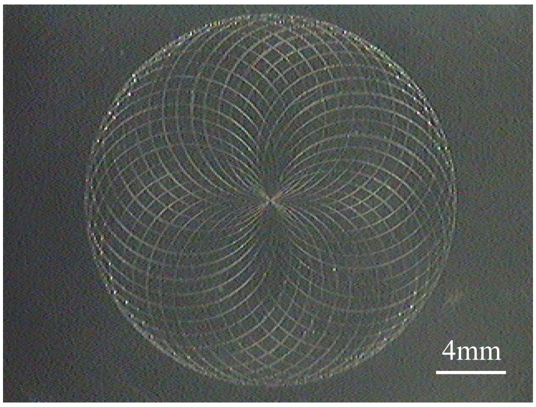

(b) $r_1 = r_2$

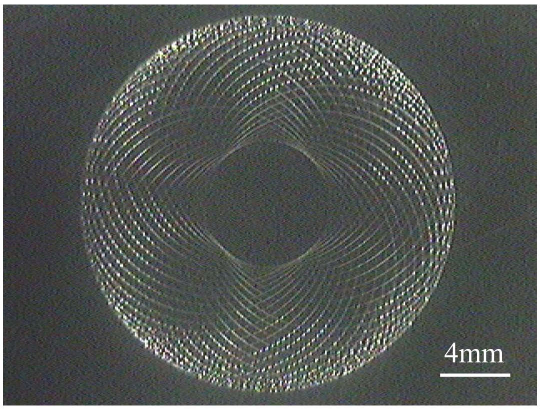

(c) $r_1 < r_2$

Fig. 7. Machining examples.

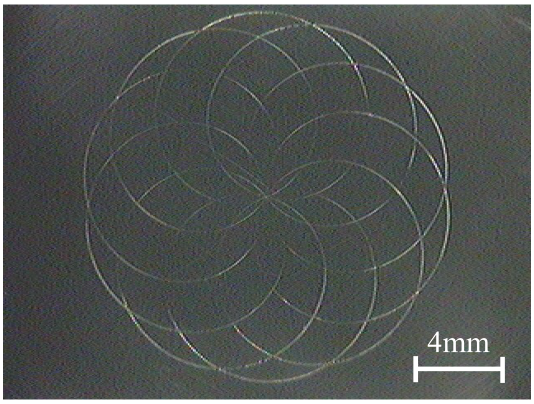

(a) Machined groove

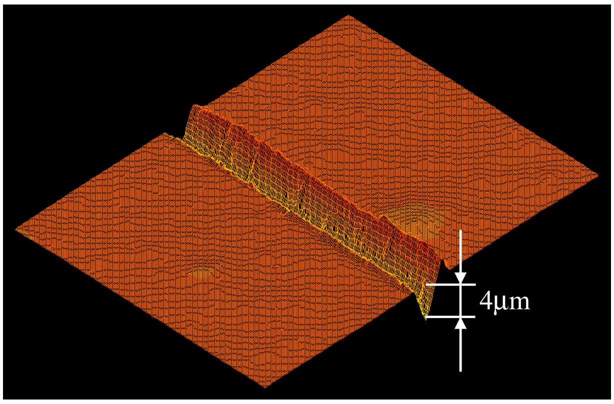

(b) Groove shape around center

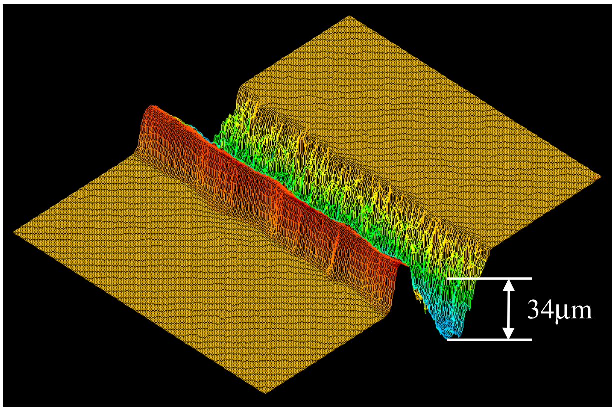

(c) Groove shape around circumference

Fig. 8. Machining without pre-polishing process.

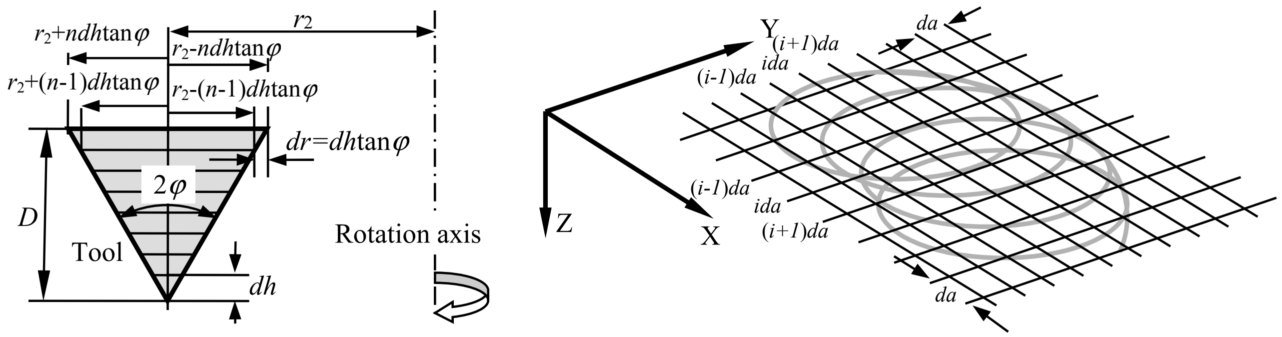

(a) Tool division (b) Surface area division

Fig. 9. Surface structure model.

ample of the machined groove in which $r_1 = r_2 = 4$ mm, $\omega_1 = 0.628$ rad/s (6 rpm), and $\omega_2 = 6.28$ rad/s (60 rpm). The depth of the cut changes during rotation because of the alignment error. The effect of polishing on reducing alignment error is verified by comparing the machined groove shown in **Fig. 8(a)** with those of **Fig. 7**. **Figs. 8(b)** and **(c)** show portions of the machined groove, as observed with a laser confocal microscope. At the edges of the machined grooves, burr formation occurs because of the ductility of the aluminum alloy. According to previous reports [19, 20], reducing the grain size of the material would effectively control burr formation.

5. Surface Structure and Surface Finish

5.1. Surface Structure Model

The functions of the surface textures depend on the shapes and alignments of the micro-scale structures. A model is presented to simulate surface structures formed by the presented texturing method. The tool is divided into n discrete segments in the height direction, as shown in **Fig. 9(a)**. When texturing is conducted with the tool of an apex angle 2φ at the depth D, the height increment dh is:

$$dh = \frac{D}{n} \quad \ldots\ldots\ldots\ldots\ldots \quad (2)$$

Because the center of the tool machines the grooves with a maximum depth D and the rotation radius r_2, the locus of each segment at the height $h_i = i \cdot dh$ $(i = 0, 1, 2, \ldots, n)$ is given as a function of time t:

$$\left.\begin{aligned} x_i &= r_1 \cos(\omega_1 t) + (r_2 + dr_i)\cos\{(\omega_1 + \omega_2)t\} \\ y_i &= r_1 \sin(\omega_1 t) + (r_2 + dr_i)\sin\{(\omega_1 + \omega_2)t\} \end{aligned}\right\} (3)$$

where $dr_i = i \cdot dh \tan\varphi$ $(i = -n, -n-1, \ldots, -1, 0, 1, \ldots, n-1, n)$. The depth at each segment d_i at the point (x_i, y_i) is given by:

$$d_i = -dh(n - |i|) \quad \ldots\ldots\ldots\ldots \quad (4)$$

where $|i|$ is the absolute value operator of the index variable i. In order to save computational memory, the surface structure is simulated here for one quarter of the texturing area. The texturing area is divided into $N \times N$ segments in the X-Y plane, as shown in **Fig. 9(b)**. Because the surface texture is fabricated with the radius $r_1 + r_2 + dr_n$, the size of the surface segment da is:

$$da = \frac{r_1 + r_2 + dr_n}{N} \quad \ldots\ldots\ldots\ldots \quad (5)$$

Therefore, the coordinates of each surface segment are assigned by $(i \cdot da, i \cdot da)$ $(i = 0, 1, 2, \ldots, N)$. The coordinates of the removal area, given by Eq. (3), are assigned by the segment index $(x_i/da,\ y_i/da)$ in the X and Y directions. The depth of the segment index is updated by the increment d_i in Eq. (4) when d_i is less than the depth stored in the memory of the computer running the simulation, where the depth of all segments is defined as 0 at the beginning of the simulation.

Figure 10 shows an example of a simulated surface structure in which r_1 and r_2 are 1.3 and 1.5 mm, respectively. Grooves of 50 μm in depth are finished at workpiece and tool spindle speeds of 20 and 400 rpm, respectively. **Fig. 11** compares the simulated surface structure with a real workpiece machined using identical cutting parameters, where the simulation results are shown for a square region of 0.5 mm on a side. The simulation agrees very well with the actual surface structure.

5.2. Effect of Tool Orientation

Because the tool used in the cutting tests is pyramidal, as shown in **Fig. 6**, consisting of four equilateral triangular faces, the tool face orientation affects both the removal process and the surface textures to be machined. Cutting tests were conducted with changes in tool face orientation. **Fig. 12** shows the surface finishes produced when the direction normal to one equilateral triangle face or one ridge of the pyramid is in the vertical plane containing the direction tangent to the tool rotation. In **Fig. 12(a)**, the equilateral triangular face acts as a rake face to form a chip. In **Fig. 12(b)**, chips form on the two inclined triangular faces. Burrs and chips are observed on the surface created with this tool orientation. Therefore, the machining manner used in **Fig. 12(a)** is recommended for a smoother surface finish. The apex angle viewed from the cutting direction is also associated with the tool orientation used in

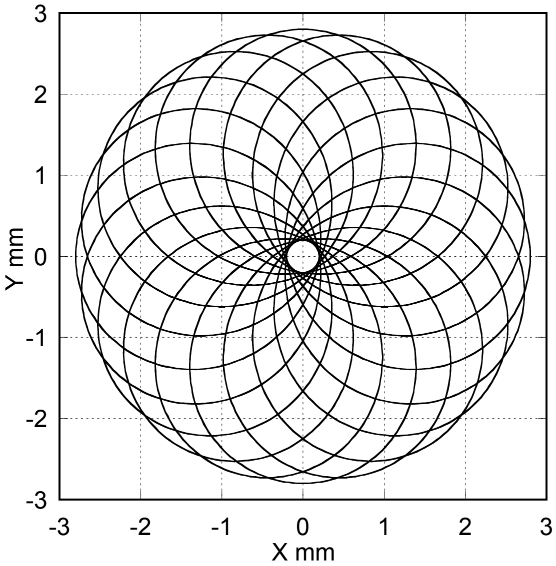

(a) Locus of tool

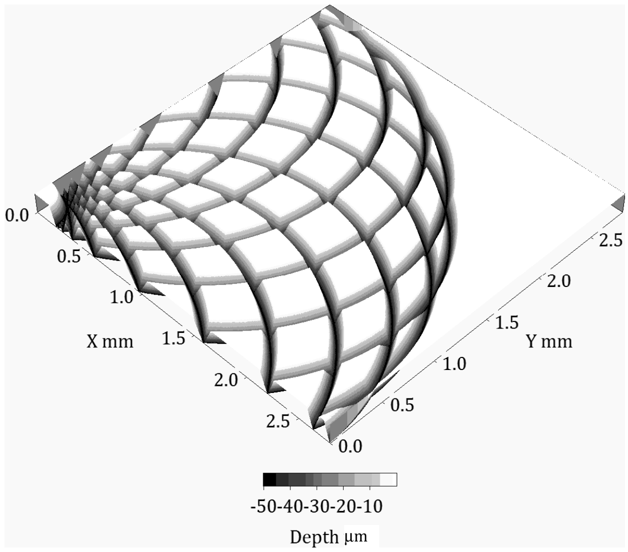

(b) Surface profile

Fig. 10. Surface structure simulation.

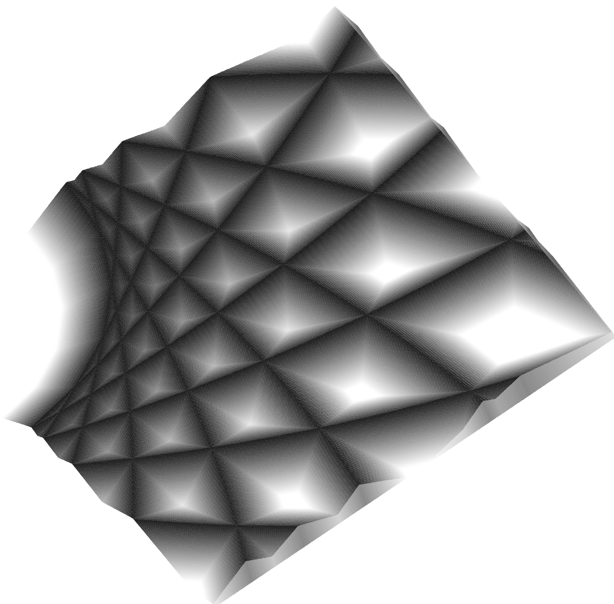

(a) Simulated structure

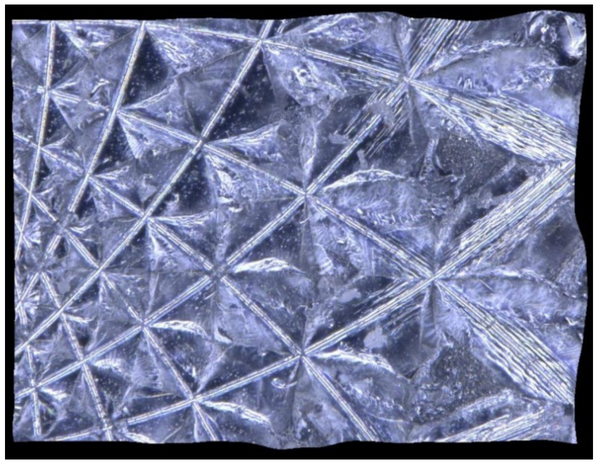

(b) Machined structure

Fig. 11. Comparison of simulated and actual machined structures.

the cutting tests. The apex angles of **Figs. 12(a)** and **(b)** are 60° and 90°, respectively. The surface structure, in turn, changes with the width of the groove. To clearly observe the effect of the apex angle, surface structures are simulated for both cases of **Fig. 12**. **Fig. 13** shows the simulation of the surface structures textured with the tool at apex angles of 60° and 90°, respectively, where the cutting parameters are identical to those in Condition B of **Table 1**. Although the surface structure is clear in machining with the tool at an apex angle of 90°, in the case of **Fig. 12(b)**, the flattened area of the structure around the workpiece center expands in **Fig. 13(a)** because the grooves overlap.

6. Cutting Force Model

6.1. Force Model in Micro Cutting of Aluminum Alloy

A force model is applied to estimate the cutting force on the aluminum alloy. In microscale cutting, the indentation force is large relative to the shearing force to form chips [21]. Therefore, the cutting force F is regarded as the sum of the indentation and shearing components [22]:

$$F = k_p S + k_c A \quad \quad (6)$$

where k_p is the specific indentation force, which is the indentation force loaded on a unit edge length. k_c is the specific shearing force, which is the shearing force loaded

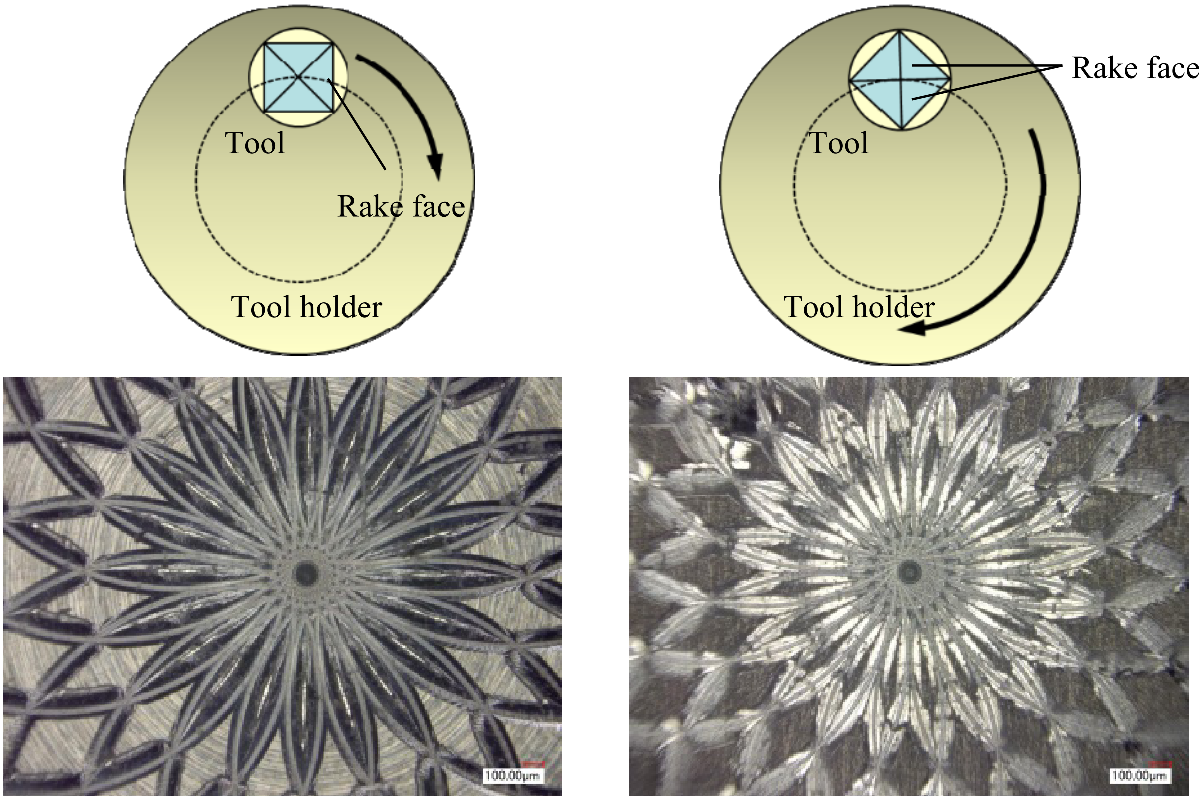

(a) One-faced tool cutting

(b) Two inclined tool faces

Fig. 12. Surface finishes.

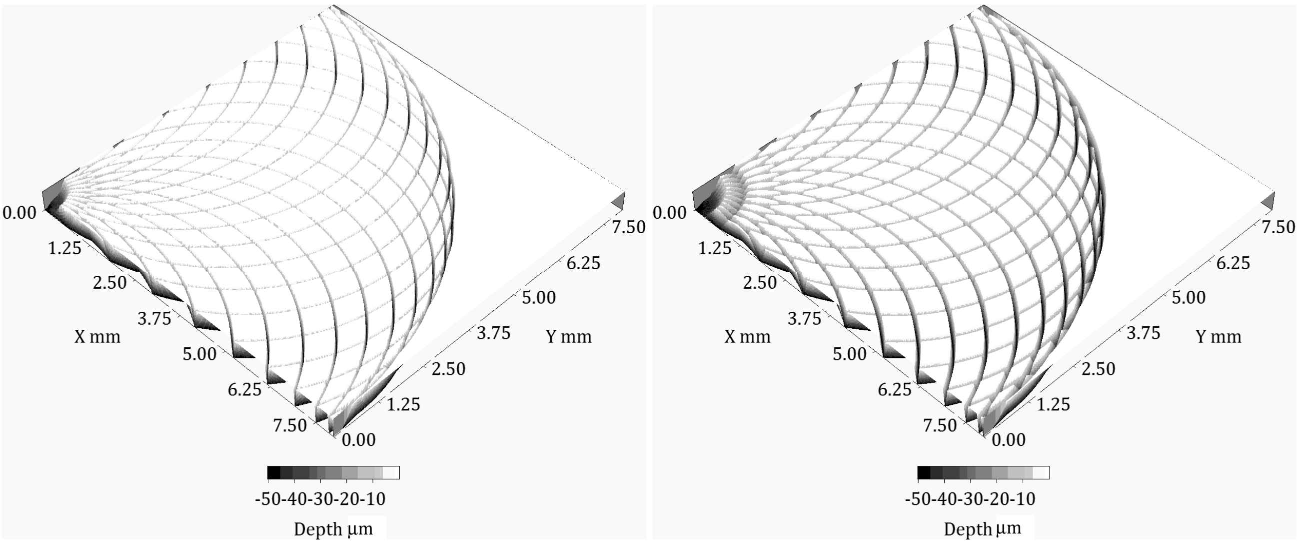

(a) Apex angle of 60° (as in **Fig. 12(a)**)

(b) Apex angle of 90° (as in **Fig. 12(b)**)

Fig. 13. Surface structures in simulation.

on a unit cutting area. S and A are the cutting edge length and the cutting area, respectively, which are associated with the depth of the cut d. When the wedge angle of the tool is 2φ, as shown in **Fig. 14**, the principal component F_P loaded on the tool in the cutting direction is:

$$F_P = k_{Pp}\frac{2d}{\cos\varphi} + k_{Pc}d^2\tan\varphi \quad \ldots\ldots\ldots \quad (7)$$

where k_{Pp} and k_{Pc} are the specific indentation and shearing forces in the cutting direction, respectively. The thrust component F_T loaded on the inclined edge in the vertical direction relative to the cutting direction is given by:

$$F_T = k_{Tp}\frac{2d}{\cos\varphi}\sin\varphi + k_{Tc}d^2\tan\varphi \quad \ldots\ldots \quad (8)$$

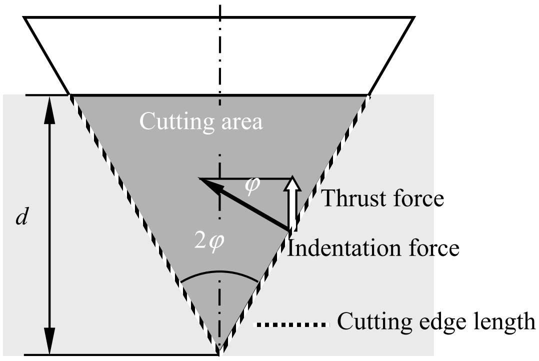

Fig. 14. Cutting area and edge length.

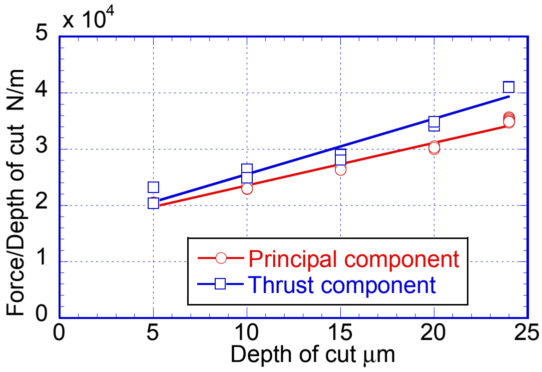

Fig. 15. Specific cutting forces for depth of cuts.

Table 2. Parameters in force model.

		Principal	Thrust
Indentation k_p	N/m	6922	13602
Shearing k_c	N/m^2	1311	1706

where k_{Tp} and k_{Tc} are the specific indentation and shearing forces, respectively.

In order to obtain k_p and k_c, cutting tests were conducted to measure the cutting force necessary for the aluminum alloy A5056. The cutting direction coincided with the direction normal to the equilateral triangular face of the tool, as in the cutting manner of **Fig. 12(a)**. The forces F_P/d and F_T/d in Eqs. (7) and (8) are expressed as:

$$\left.\begin{aligned}\frac{F_P}{d} &= k_{Pp}\frac{2}{\cos\varphi} + k_{Pc}d\tan\varphi \\ \frac{F_T}{d} &= k_{Tp}\frac{2}{\cos\varphi}\sin\varphi + k_{Tc}d\tan\varphi\end{aligned}\right\} \quad \cdots \quad (9)$$

Figure 15 shows the change in F_P/d and F_T/d with the depth of cut d. From this figure, k_p and k_c in the principal and thrust components, respectively, are determined, as shown in **Table 2**. Because the rake angle is negative, the thrust component becomes large relative to the principal force.

6.2. Cutting Force Simulation

The cutting parameters should be determined properly by estimating the cutting force loaded on the tool and the texturing machine. Because the cutting force cannot be measured on the developed machine, periodic changes in the cutting force with the rotations of the tool holder are estimated in the simulation, based on the force model acquired in the planing test here. A simplified model is applied to the cutting force simulation under the following assumptions:

(1) The changes in the cutting force at groove intersections are ignored.

(2) Only the side edge of the tool cuts the material when the machined grooves are close to each other, such as at the workpiece center in Condition B of **Table 1**. The other side edge does not cut. The changes in the cutting force near the workpiece center are ignored.

(3) Burr formation occurs in the actual machining, as shown in **Fig. 8**. The model does not consider the influence of burr formation on the cutting force.

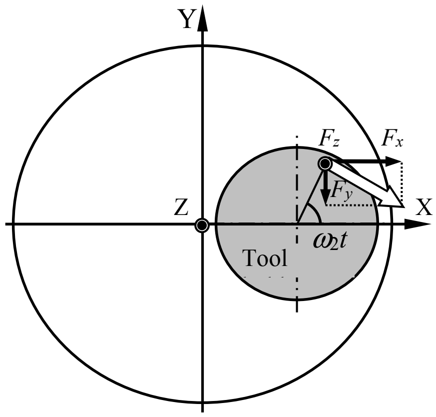

Fig. 16. Coordinate system.

Although the model does not simulate the cutting force changes due to the surface structures fabricated by the prior cutting, the maximum force may be estimated in determining the cutting parameters.

As an example, the cutting force is simulated for the cutting parameters in Condition B of **Table 1**, where the depth of the cut is controlled to increase continuously with increased cutting time. The determined parameters of **Table 2** in the force model are used to obtain the principal and thrust components. **Fig. 16** shows the coordinate system for the force loaded on the tool.

The time T for one rotation of the workpiece is:

$$T = \frac{2\pi}{\omega_1} \quad \cdots \quad (10)$$

Fig. 17 shows the changes in cutting areas with cutting time. When the cutting time t is less than T, the cutting tool penetrates the workpiece and the cutting area changes with the cutting depth, as shown in **Fig. 17(a)**. The tool removes the same amount of material every ω_2/ω_1 rotations. Therefore, the cutting area is determined by both the cutting position and the removal shape machined in the previous cutting after the cutting time T, as shown in

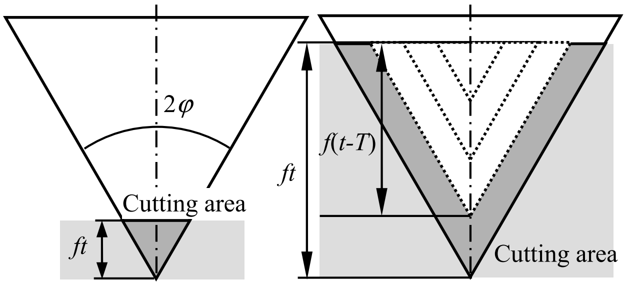

Fig. 17. Cutting areas.

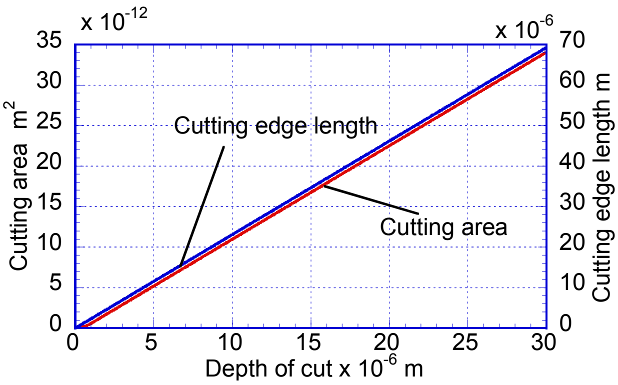

Fig. 18. Cutting areas and edge lengths for depth of cut.

Fig. 17(b). The change in the cutting area A as a function of time t is:

$$A = \begin{cases} f^2t^2 \tan\varphi & (t \leq T) \\ f^2t^2 \tan\varphi - f^2(t-T)^2 \tan\varphi & (t > T) \end{cases} \quad (11)$$

The cutting edge length S at time t is:

$$S = \frac{2ft}{\cos\varphi} \quad \ldots\ldots\ldots\ldots (12)$$

Because the principal and the thrust components are given by Eqs. (7) and (8), the X, Y, and Z components in the cutting force are:

$$\left.\begin{aligned} F_x &= F_P \sin(\omega_2 t) \\ F_y &= -F_P \cos(\omega_2 t) \\ F_z &= F_T \end{aligned}\right\} \quad \ldots\ldots\ldots (13)$$

Figure 18 shows the change in the cutting area and the cutting edge length with increasing the depth of cut to 30 μm. The X, Y, and Z components of the cutting force are simulated as a function of cutting time, as shown in **Fig. 19**. **Fig. 20** shows the changes in the cutting force at depths d of 10 and 20 μm. Because the tool rotates during the cutting, the X and Y components of the force, which depend on the principal component, change with the tool orientation. Meanwhile, the Z component of the cutting force increases monotonically with increased cutting depth and thrust component. As described in the assumptions used in the simulation, the model ignores the changes in the cutting force with the surface structure fabricated by prior cutting. In the actual machining process, each component changes according to the intersections of the grooves. However, the maximum force estimated in the simulation can be used to determine the cutting parameters properly, considering the torque limitations of the servomotors on the cutting machine.

7. Conclusions

A parametric texturing method has been presented to fabricate periodic circular structures on the surface of a substrate by the simultaneous rotation of the workpiece and cutting tool. The texturing patterns are controlled by four parameters: the distance from the rotation center of the workpiece to that of the tool holder, the rotation radius of the tool, and the angular velocities of the workpiece and the tool holder. The machining patterns can be simulated numerically using mathematical equations according to the specified control parameters. Because the presented machining method requires no NC programs, the periodic patterns can be changed easily by adjusting the control parameters.

A texturing machine was constructed to perform the presented process. In the texturing, polishing of the workpiece with pads mounted on the tool holder is required to minimize the alignment error before machining. The workpiece surface is finished such that the distance between the tool and workpiece is uniform throughout the texturing area.

A model was presented for controlling the surface structure by adjusting the cutting parameters. The model considers the tool geometry to simulate the structure shapes formed on the surface. The effect of the tool orientation on the surface finish was discussed to provide improved surface quality. When the equilateral triangular tool face acts as a rake face to form a chip, the surface structures can be finished without the formation of burrs or chips.

A force model is discussed for the cutting of the aluminum alloy. Because the employed tool has a large negative rake angle, the thrust force becomes large. In the microscale cutting, the indentation force is included in the force model. The force model is determined considering both the shearing and indentation forces.

The cutting force is simulated to determine the cutting parameters, considering the torque limits of the servomotors in the texturing machine. The cutting force increases continuously with the depth of the cut. The X and Y components of the cutting force change with the tool orientation; the Z component increases monotonically with the depth of cut. The maximum force components during one workpiece rotation can be used in the process design.

References:

[1] R. L. Wenzel, "Resistance of Solid Surfaces to Wetting by Water," Industrial and Engineering Chemistry, Vol.28, No.8, pp. 988-994, 1936.

[2] A. B. D. Cassie and S. Baxter, "Wettability of Porous Surfaces," Trans. Faraday Soc., Vol.40, pp. 546-551, 1944.

[3] A. A. G. Bruzzone, H. L. Costa, P. M. Lonardo, and D. A. Lucca,

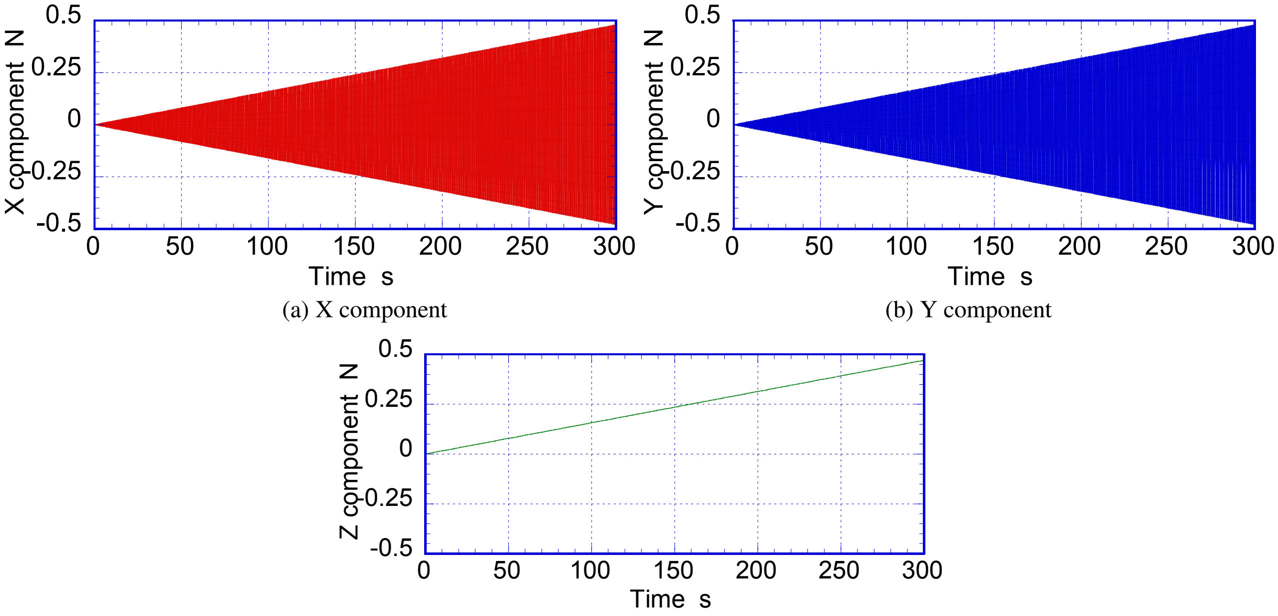

(a) X component
(b) Y component
(c) Z component

Fig. 19. Cutting force components.

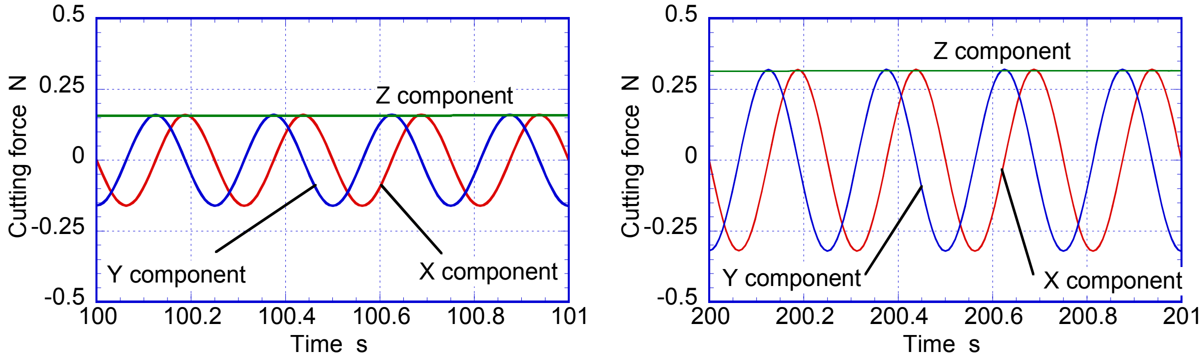

(a) Cutting depth, 10 m
(cutting time, 100-101 s)

(b) Cutting depth, 20 m
(cutting time, 200-201 s)

Fig. 20. Changes in cutting force.

"Advances in Engineered Surfaces for Functional Performance," CIRP Annals – Manufacturing Technology, Vol.57, pp. 750–769, 2008.

[4] M. Wakuda, Y. Yamauchi, S. Kanzaki, and Y. Yasuda, "Effect of Surface Texturing on Friction Reduction between Ceramic and Steel Materials under Lubricated Sliding Contact," Wear, Vol.254, pp. 356–363, 2003.

[5] P. Basnyat, B. Luster, C. Muratore, A. A. Voevodin, R. Haasch, R. Zakeri, P. Kohli, and S. M. Aouadi, "Surface Texturing for Adaptive Solid Lubrication," Surface & Coatings Technology, Vol.203, pp. 73–79, 2008.

[6] F. Meng, R. Zhou, T. Davis, J. Cao, Q. W. Jane, H. Diann, and L. Jordan, "Study on Effect of Dimples on Friction of Parallel Surfaces under Different Sliding Conditions," Applied Surface Science, Vol.256, pp. 2863–2875, 2010.

[7] A. A. Voevodin and J. S. Zabinski, "Laser Surface Texturing for Adaptive Solid Lubrication," Wear, Vol.261, pp. 1285–1292, 2006.

[8] D. P. Wan, B. K. Chen, Y. M. Shao, S. L. Wang, and D. J. Hu, "Microstructure and Mechanical Characteristics of Laser Coating – Texturing Alloying Dimples," Applied Surface Science, Vol.255, pp. 3251–3256, 2008.

[9] X. Luo, Y. Wang, P. Chen, and L. Zhou, "Investigation of CO_2 Laser Beam Modulation by Rotating Polygon," Optics and Lasers in Engineering, Vol.49, pp. 132–136, 2011.

[10] M. Yoshino, T. Matsumura, N. Umehara, Y. Akagami, S. Aravindan, and T. Ohno, "Engineering Surface and Development of a New DNA Micro Array Chip," Wear, Vol.260, pp. 274–286, 2006.

[11] T. Matsumura, F. Iida, T. Hirose, and M. Yoshino, "Micro Machining for Control of Wettability with Surface Topography," Journal of Materials Processing Technology, Vol.212, pp. 2669–2677, 2012.

[12] Y. Q. Wang, G. F. Wu, Q. G. Han, L. Fang, and S. R. Ge, "Tribological Properties of Surface Dimple-textured by Pellet-pressing," Procedia Earth and Planetary Science, Vol.1, pp. 1513–1518, 2009.

[13] T. Matsumura, M. Serizawa, T. Ogawa, and M. Sasaki, "Surface Dimple Machining in Whirling," Journal of Manufacturing Systems, DOI: 10.1016/j.jmsy.2014.07.008, 2014 (in press).

[14] S. Kogusu, T. Ishimatsu, and Y. Ougiya, "Rapid Generation of Surface Dimples Using End Milling," International Journal of Automation Technology, Vol.1, pp. 45–51, 2007.

[15] T. Matsumura and S. Takahashi, "Micro Dimple Milling on Cylinder Surfaces," Journal of Manufacturing Processes, Vol.14, pp. 135–140, 2012.

[16] E. Graham, C. I. Park, and S. S. Park, "Inclined Ball End Milling of Micro-Dimpled Surfaces for Polymeric Components," Proceedings of 41th North American Manufacturing Research Conference, Vol.41, NAMRC41-1591, 2013.

[17] T. Matsumura and S. Takahashi, "Machining of Micro Dimples in Milling for Functional Surfaces," American Institute of Physics, Proceedings of the 14th International ESAFORM Conference on Material Forming, Vol.1353, pp. 567-572, 2011.

[18] T. Matsumura and M. Kakishita, "Parametric Glass Milling with Simultaneous Control," Journal of Manufacturing Processes, Vol.15, pp. 1–7, 2013.

[19] T. Komatsu, T. Matsumura, and S. Torizuka, "Effect of Grain Size in Stainless Steel on Cutting Performance in Micro-Scale Cutting," International Journal of Automation Technology, Vol.5, No.3, pp. 334–341, 2011.

[20] T. Komatsu, Y. Musha, T. Yoshino, and T. Matsumura, "Surface Finish and Affected Layer in Milling of Fine Crystal Grained Stainless Steel," Journal of Manufacturing Processes, Vol.19, pp. 148-154, 2015.

[21] J. Chae, S. S. Park, and T. Freiheit, "Investigation of Micro-cutting Operations," International Journal of Machine Tools & Manufacture, Vol.46, pp. 313–332, 2006.

[22] H. Perez, A. Vizan, J. C. Hernandez, and M. Guzman, "Estimation of Cutting Forces in Micromilling through the Determination of Specific Cutting Pressures," Journal of Materials Processing Technology, Vol.190, pp. 18–22, 2007.

Name:
Takashi Matsumura

Affiliation:
Professor, Mechanical Engineering, Tokyo Denki University

Address:
5 Senjyu Asahi-cho, Adachi-ku, Tokyo 120-8551, Japan

Brief Biographical History:

1987-1992 Research Associate, Tokyo Institute of Technology
1992- Professor, Tokyo Denki University
1997-2006 Visiting Scholar, Massachusetts Institute of Technology

Main Works:

• T. Matsumura and T. Ono, "Cutting process of glass with inclined ball end mills," J. of Material Processing Technology, Vol.200, pp. 356-363, 2008.
• T. Matsumura, Y. Miyahara, and T. Ono, "Dynamic characteristics in the cutting operations with small diameter end mills," J. of Advanced Mechanical Design, Systems, and Manufacturing, Vol.2, No.4, pp. 609-618, 2008.
• T. Matsumura, K. Minai, and Y. K. Rong, "Micro glass milling on multi-axis machine tool," Trans. of the North American Manufacturing Research Institution of SME, Vol.37, pp. 205-212, 2009.
• T. Matsumura and E. Usui, "Predictive cutting force model in complex-shaped end milling based on minimum cutting energy," Int. J. of Mach. Tools and Manufact., Vol.50, No.5, pp. 458-466, 2010.

Membership in Academic Societies:

• Japan Society of Mechanical Engineers (JSME)
• Society of Automotive Engineers of Japan (JSAE)
• Society of Materials Science, Japan (JSMS)
• Japan Society for Abrasive Technology (JSAT)
• Japan Society for Precision Engineering (JSPE)
• Society of Manufacturing Engineers (SME)